ELSEVIER

Thermochimica Acta 347 (2000) 53–61

thermochimica acta

www.elsevier.com/locate/tca

Applicability of 8OCB for temperature calibration of temperature modulated calorimeters

C. Schick[a,*], U. Jonsson[b], T. Vassiliev[c], A. Minakov[d], J. Schawe[e], R. Scherrenberg[f], D. Lőrinczy[g]

[a]*University of Rostock, Department of Physics, Universitätsplatz 3, D-18051 Rostock, Germany*
[b]*Umeå University, Applied Physics and Electronics, S-901 87 Umeå, Sweden*
[c]*Institute of Physical Chemistry, Bulgarian Academy of Sciences, BG-1113 Sofia, Bulgaria*
[d]*General Physics Institute, Vavilov st. 38, 117942 Moscow, Russia*
[e]*IFA GmbH, Schillerstr. 18, D-89077 Ulm, Germany*
[f]*DSM Research B.V., Koestraat 1, NL-6167 RA, Geleen, The Netherlands*
[g]*Department of Biophysics, University Medical School of Pécs, Szigeti str. 12, H-7643 Pécs, Hungary*

Received 5 August 1999; accepted 26 August 1999

Abstract

Calibration of temperature modulated calorimeters (TMC) is essential because it is often not possible to calculate heat capacity and sample temperature directly from the quantities measured. The question arises whether temperature calibration used in conventional calorimetry is also valid for TMC's. To prove this, a well defined transition is needed which does not disturb the temperature profile within the sample during modulation. The response of the whole system (calorimeter, sample, transition) must be linear. Some low energy liquid crystal transitions behave in this way, under certain conditions, and can be used for temperature calibration in TMC's. The procedure is demonstrated for the nematic to smectic-A transition in a cyanobiphenyl liquid crystal (8OCB). The applicability of 8OCB for temperature calibration is shown for temperature modulated DSC, AC calorimeter, 3ω method and photo-acoustic method.

Keywords: Temperature calibration; Temperature modulated calorimetry; Complex heat capacity; Liquid crystal; Phase transition

1. Introduction

To measure complex heat capacity as a function of temperature or time and frequency is one of the most interesting application of modern calorimetric techniques. With introduction of the so-called 3ω method by Birge and Nagel [1], it was shown that heat capacity spectroscopy can be performed [2]. To enlarge frequency range available, is one of the main problems in the refinement of heat capacity spectroscopy like in dielectric spectroscopy. The 3ω-method is mainly used because it covers several orders of magnitude in frequency. The 3ω-method can be used up to frequencies in the order of 100 kHz, as recently shown by Birge [3]. The method needs a large sample thickness compared to the thermal wavelength. For higher frequencies this is easily attained, but for frequencies below 0.1 Hz care must be taken not to violate the fundamental conditions of the method. In

* Corresponding author. Tel.: +49-381-498-1644; fax: +49-381-498-1626.
E-mail address: christoph.schick@physik.uni-rostock.de (C. Schick).

0040-6031/00/$ – see front matter
PII: S0040-6031(99)00416-5

photo-acoustic techniques [4] which can be used also up to kHz region to determine complex heat capacity sample thickness compared to thermal wavelength can vary form thin to thick limits. However, if the sample under study has low thermal conductivity one usually measure at thermally thick limit as in 3ω-method.

If one wants to expand the frequency range to lower frequencies, it is often better to use methods where the sample should be thin compared to thermal wavelength. This assumption is valid in AC calorimetry [5] and temperature modulated DSC (TMDSC) [6]. The combination of different calorimetric spectroscopy methods gives complex heat capacity for more than seven orders of magnitude in frequency [7]. But if one wants to combine different techniques using different apparatuses one has to calibrate the instruments carefully. In the present paper, we focus on temperature calibration of the different calorimeters used in this study. Calibration of complex heat capacity, especially that of imaginary part, is important too but it is not the aim of this paper.

2. Experimental

The nematic to smectic-A transition (N–SmA) of 4,4′-*n*-octyloxycyanobiphenyl (8OCB)[1] was investigated for use as a potential calibration standard for AC calorimetry, 3ω-method, photo-acoustic and TMDSC. A description of the different techniques can be found in [1,4,5,8], respectively. Some overviews are given in several papers in [9].

Temperature calibration in conventional calorimetry, means the calibration of the thermometer by taking the thermal lag between thermometer and sample into account [10–12]. Compensation for thermal lags is achieved when the calorimeter is calibrated at zero heating rate and the indicated temperature is extrapolated to zero heating rate. This procedure, recommended by GEFTA [10], results in reproducible calibration independent of the type of calorimeter. Thus in everyday use, the heating rate dependence of the measured temperature must be considered. In the case of TMC's we must take into account, not only the effect of the underlying heating rate q_0 but also possible influences of the DC component due to AC heating and other possible errors arising from the extensive numerical calculations and averaging procedures used in the data treatment. It is essential to calibrate, not only the thermometer but also the temperature scale for the different quantities measured in a TMC experiment.

It is well known that the calorimetric response is not always linear [13]. This is especially true for sample reactions with non-linear temperature responses, e.g., narrow phase transitions proceeding at isothermal conditions. From a theoretical description of classical scanning calorimeters we can derive rules to get correct values, e.g., of melting temperatures [14,15]. The most common procedure gives a construction for the 'peak onset temperature'. This construction is the basis of temperature calibration in conventional DSC where materials with well-defined first order phase transitions are used [10,11].

Because of the Fourier analysis used in the TMC data evaluation technique it is not so easy to correct for a possible non-linear response of the calorimeter. The 'peak onset temperature' becomes meaningless, as the prerequisites for the construction procedure are not fulfilled in TMC's. Here is no linearly increasing heat transfer into the sample established. In a TMC we have to choose a phase transition for temperature calibration which gives a linear response all over the transition range.

Therefore, we need a phase transition which follows the modulation and leads to linear behaviour for the whole system. This should be achieved by a second-order transition. It was shown by AC calorimetry [16,17] and volumetric measurements [18] that the nematic to smectic-A transition of 8OCB is of second order. Because there is no latent heat, we expect linear behaviour which also was confirmed by TMDSC [19].

3. Results

First, the phase behaviour of 8OCB, used as received from Merck (see Footnote 1), was investigated on heating and cooling by using a Perkin–Elmer DSC-7 and a Setaram Micro DSC-II and a DSC-121. The calorimeters were used in the conventional (DSC) mode. From these measurements, the reproducibility of the peak maximum temperature and the stability of the sample were tested. The nematic to smectic-A

[1] Available as M24 from: Merck KgaA, Darmstadt, Germany.

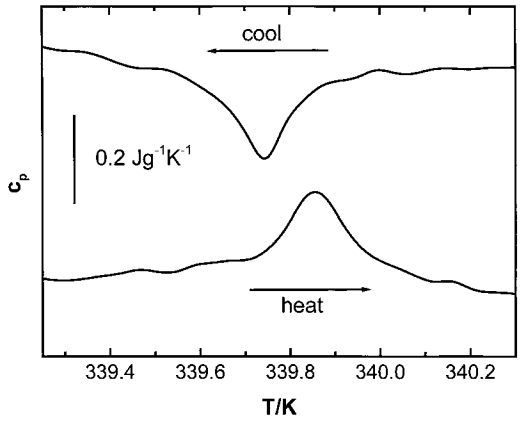

Fig. 1. The N–SmA transition of 80CB on 0.05 K min^{-1} cooling/heating rate done by Setaram Micro DSC-II. Sample mass: 77.3 mg.

transition of 8OCB is of second order. Therefore, to determine the temperature of the phase transition the peak maximum has to be used instead of the peak onset temperature which has to be used for first-order transitions. Because the observed peak in a DSC experiment is very small, i.e., ≈0.3 kJ kg^{-1}, the additional deviation between sample temperature and oven temperature is negligible due to the small increase of heat flow. It was shown that peak temperature is reproducible within 0.2 K over several heating and cooling cycles. Thus, the accuracy is high enough to perform temperature calibration of different equipments. A DSC scan at low scanning rate is shown in Fig. 1. Experimental details about the Setaram Micro DSC-II can be found in [20]. The observed temperature difference, of about 0.1 K between peak maximum, from heating and cooling is due to thermal lag. Extrapolation to zero heating and cooling rate results in equal peak temperatures of 339.8 K, see also [19,21].

Unfortunately, 8OCB cannot be recommended for absolute temperature calibration because transition temperature depends on purity.

Next, we studied the nematic to smectic-A transition in 8OCB by using different temperature modulated calorimeters. The different calorimeters were a 3ω-spectrometer designed by Jonsson [22], an AC calorimeter designed by Minakov [23], a photo-acoustic apparatus constructed by Vassiliev [24,25] and five different TMDSC (Perkin–Elmer DSC-7 and Pyris 1 DSC, TA Instruments DSC 2920, Mettler DSC 821, Setaram DSC 121).

3.1. 3ω method

In 1985 Birge and Nagel [1] introduced heat capacity spectroscopy in which the sample was probed by using a sinusoidally varying temperature. In this case, one obtains the product of the thermal conductivity κ, and the complex specific-heat capacity per unit volume c_p^* of a sample. In order to measure complex specific-heat capacity, Birge and Nagel [2] used a method which is generally referred to as the 3ω-method.

The 3ω-method for measuring complex heat capacity is based on the principle of using a thin (ca. 0.1 μm) metallic strip as both heater and thermometer. A sinusoidally varying current of frequency ω is supplied to the heater, which is located on the surface of the sample. For a liquid sample, the heater is placed on a substrate which is submerged in the liquid. The electrical power input to the heater consists of dc- and ac-components, where the latter dissipates into the sample through thermal waves of frequency 2ω. A measured ac-voltage over the heater gives an amplitude modulated signal, with components at frequency ω and 3ω. The amplitude of the signal at 3ω yields the temperature oscillation of the heater, which depends on the thermal properties of the sample.

The ideal planar heater model [26] assumes an infinitely thin heater with a constant amplitude of the temperature oscillation throughout its whole area. However, in a practical situation, the alternating electric current in the heater leads to a dc-heating that causes a temperature rise ΔT_h, of the heater above the ambient temperature T_{amb}. For a high heater power, a temperature gradient ΔT_{grad} arises in the heater. As a consequence, a peak in the heat capacity associated with a transition will be broadened. Furthermore, this dc-heating creates a temperature gradient in the sample as well. This makes it difficult to determine the sample temperature and, therefore, transition temperatures. To understand how the design of the heater and the construction of the sample cell influences the temperature scale and the width of a transition peak, the nematic to smectic-A transition in the liquid crystal 8OCB has been studied. In Fig. 2, κc_p as a function of temperature for 8OCB is shown. Here c_p is

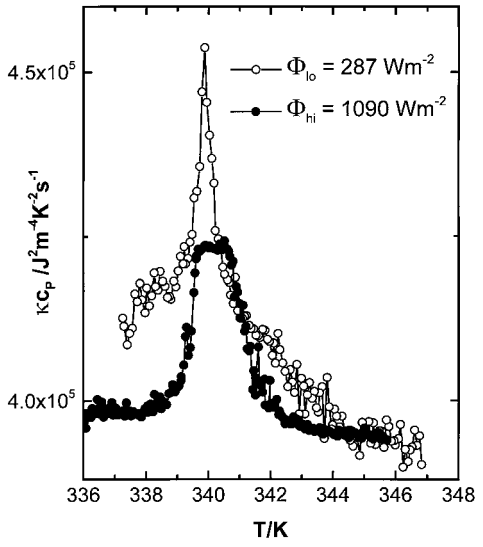

Fig. 2. The N–SmA transition in 8OCB plotted for two different values of heat flow. The temperature scale is corrected for the effect of temperature gradients. The $\Phi_{hi} = 1090\ W\ m^{-2}$ curve is broadened and has a lower peak relative to the Φ_{lo}=287 W m^{-2} curve due to a larger temperature gradient in the heater.

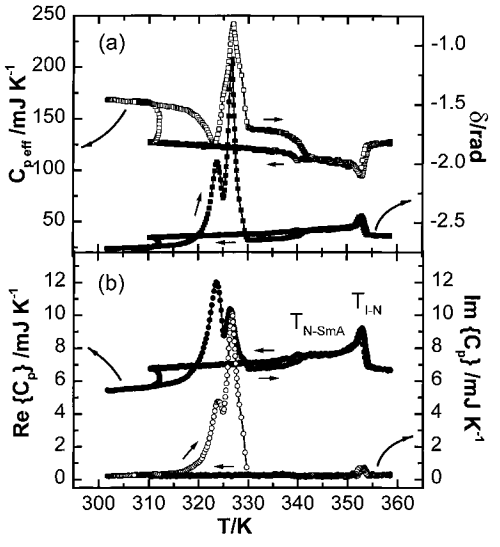

Fig. 3. Temperature dependencies of the effective heat capacity C_{eff} and the phase shift d (a) as well as of the Re$\{C_p(T)\}$ and Im$\{C_p(T)\}$parts (b) of the 8OCB sample of thickness 0.3 mm. The measurements were performed at the underlying heating–cooling rate 3 K min^{-1}, the modulation frequency f=1 Hz, the heat-flow amplitude P_0=9.2 mW and the temperature modulation amplitude T_A ca. 0.035 K.

the modulus of complex specific heat capacity per unit volume and κ the thermal conductivity. For details of the measurement and the equipment used, see [22].

3.2. AC calorimetry

The liquid crystal 8OCB was extensively studied by AC calorimetry [16,17]. Results for the sample used in this study are shown in Figs. 3 and 4. Details about the calorimeter and the data treatment algorithm can be found in [23,27].

The calorimeter-cell, i.e., the system for creation and registration of temperature modulation in a disk-shaped sample, consists of a heater, a sensor, and a holder. Thus, the system consists of four layers, including the sample. As it was shown in [27], the sample heat capacity C_p and the thermal conductivity κ, can be calculated from the measured temperature amplitude and phase. Before measuring, the empty cell has to be calibrated.

The sample was placed between two polished sapphire substrates — the sensor and the heater, respectively — without any cuvette. The sample was melted to obtain good thermal contact to the substrates. Small glass posts at three points fixed the distance between the substrates. Pressure was then applied to this sandwich with a thin silk thread. The shape of the melted sample was stable due to the surface tension force. The sample thickness d was equal to 0.3 mm, the area

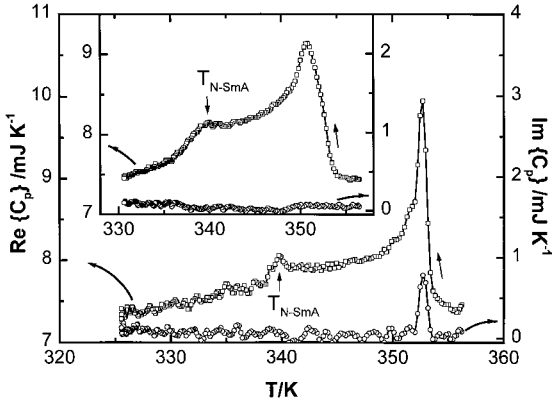

Fig. 4. Temperature dependencies of the real (Re) and the imaginary (Im) parts of heat capacity for the same sample as in Fig. 3. The measurements were performed at f=1 Hz, P_0=5.1 mW and T_A ca. 0.02 K. The same curves at relatively large modulating amplitudes P_0=20.3 mW and T_A ca. 0.1 K are shown in the insert.

S=7 mm^2 and the sample volume was about 2×10^{-3} cm^3. Though the liquid crystal 8OCB has relatively low thermal conductivity, $\kappa\approx0.3$ W m^{-1} K^{-1}, the heat flux through the sample can produce a noticeable temperature difference between the two sample faces. This temperature difference ΔT_h should be taken into account. It can be estimated as $\Delta T_h=(P_0 d)/(2S\kappa)$, $\Delta T_h/P_0\approx0.1$ K m^{-1} W^{-1}. Thus, the average sample temperature equals $T=T_S+\Delta T_h/2$, where T_S is the temperature measured by the sensor. The experiments were performed with P_0 in the range of 2–20 mW and $\Delta T_h/2$ was varied between 0.1 and 1 K.

The time lag of the heat transfer through the sample can be estimated as $\tau=(C_p d)/(S\kappa)\approx1$ s. The apparatus time lag τ_a, in our experiments, was dependent of the selected output filter time constant of the lock-in amplifier. The value of τ_a was selected to be 5 s at f=0.2–0.4 Hz and 2 s at higher frequencies, where $f=\omega/2\pi$ is the frequency of the temperature modulation. Thus, the apparatus dominated the time lag in our measurements. The time lag due to the heat transfer through the sample can be neglected.

The measurements were performed in the regions of nematic to smectic-A, isotropic to nematic and melting transitions at a heating and cooling rate of about 3 K min^{-1}. The heating and the cooling curves were reproducible after one heating–cooling cycle. Temperature dependencies of the effective heat capacity C_{eff} and the phase shift φ at frequency f=1 Hz are shown in Fig. 3a. In this case, the phase shift φ is far from zero which indicates that the sample temperature modulations are not quasi-static. First, using the algorithm described in [27], we determined the thermal conductivity of the sample at temperatures not affected by the phase transitions. We then extrapolated a function, $\kappa(T)$, to these values to cover the whole temperature range. The function $\kappa(T)$ was in good agreement with values of φ measured by a steady-state method. Then, by using the same algorithm [27] the temperature dependencies of the real, Re$\{C_p(T)\}$, and imaginary, Im$\{C_p(T)\}$, part of the sample heat capacity were determined. Plots of Re$\{C_p(T)\}$ and Im$\{C_p(T)\}$ versus temperature are shown in Fig. 3b. The transitions at nematic to smectic-A, $T_{N–SmA}$, and isotropic to nematic, $T_{I–N}$, temperatures are well defined and at the same positions (with an accuracy of about 1 K) as it was observed by Hensel et al. [19]. The difference of about 1 K may be attributed to the error of the AC calorimeter calibration. A very large peak in Im$\{C_p(T)\}$ is observed in the melting region. In this region the sample heat capacity is complex due to the excess heat capacity related to the latent heat. As shown in Fig. 3b, Im$\{C_p(T)\}$ is of the same magnitude as Re$\{C_p(T)\}$ at the end of the melting process, when the melting is mainly non-reversing. The excess heat capacity appeared only while heating, when the melting process could be modulated. When cooling, this contribution fully disappeared due to the super cooling effect. The fast crystallisation with the latent heat release and the fast spontaneous sample heating was observed at about 310 K.

Well defined steps and peaks in $C_p(T)$ at $T_{N–SmA}$ and $T_{I–N}$ were observed. These results were independent of temperature modulation amplitudes T_A below 0.1 K and no frequency dependence was observed for frequencies in the region 0.2–4 Hz. The observed value of $T_{I–N}$ depends on the underlying scanning rate as shown in Fig. 3. This dependence can be attributed to the apparatus time lag τ_a (characterised by the low pass filter in the lock-in amplifier). The transitions becomes smeared at P_0=20.3 mW and with T_A=0.1 K, as shown in the inset of Fig. 4. In this case, the temperature difference ΔT_h=2 K across the sample is relatively large. A peak in Im$\{C_p(T)\}$ is observed at the nematic-isotropic but not at the smectic-A to nematic transition, as shown in Fig. 4 for T_A=0.02 K. This peak cannot be observed at higher amplitudes $T_A\geq0.1$ K, as shown in the inset of Fig. 4.

In conclusion, it is shown that the position of the weak nematic to smectic-A transition is independent of the frequency in the range 0.2–4 Hz and the temperature modulation amplitude in the range 0.01–0.1 K. Thus, the nematic to smectic-A transition can be used for the temperature calibration of the AC calorimeter if the time (thermal) lag is considered for scan measurements.

3.3. Combined photoacoustic–differential scanning calorimeter cell (PA–DSC)

The 8OCB liquid crystal was successfully used for temperature calibration on heating and cooling of a combined PA–DSC cell [28] as well as of a variable temperature PA cell [25,29]. In Fig. 5, the PA amplitude and phase shift is shown with a 5 K min^{-1}

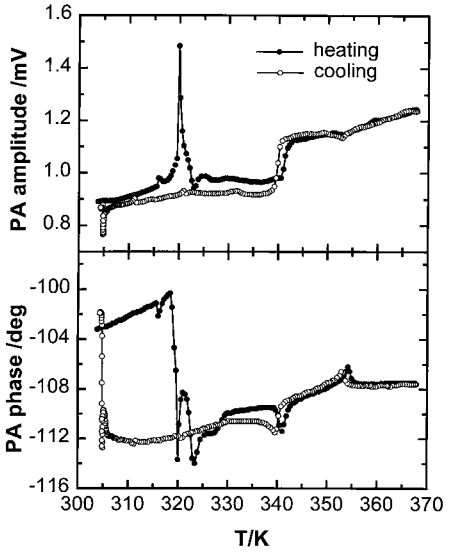

Fig. 5. PA amplitude and PA phase shift measured on heating (solid circles) and cooling (open circles) with 5 K min^{-1}, chopped frequency 63 Hz, laser beam power 34 mW.

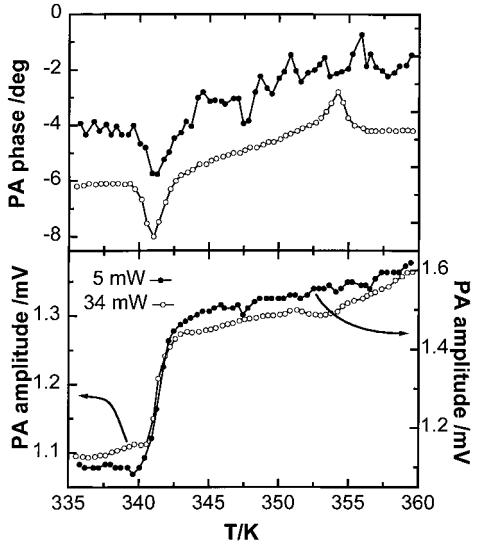

Fig. 6. PA amplitude and PA phase shift in the region of N–SmA transition measured on heating with 5 K min^{-1} and chopped frequency 63 Hz, laser beam power 5 mW (solid circles), 34 mW (open circles). Note that right and left axes for PA amplitude are different.

heating and cooling rate of the 8OCB sample. The measurements were carried out with variable temperature PA cell with a modulation frequency f=63 Hz and laser beam power of 34 mW. The regions of the three phase transitions are readily seen. Multiple melting that depend on the thermal prehistory around 320 K is associated with a maximum in the PA amplitude and a step down in amplitude is followed by a peak minimum in the PA phase shift. The N–SmA transition, at 341 K, is characterised by a step up both in the PA amplitude and phase shift, while the I–N transition at 354 K shows a peak minimum and peak maximum in the PA amplitude and PA phase shift, respectively. The differences in the N–SmA and I–N transition temperatures when heating compared to cooling is due to thermal lag.

The influence of different experimental conditions on the PA signal was tested. Measurements were performed with different scanning rates, samples of different thickness, different laser beam powers and modulation frequencies. It was found that the sample thickness and modulation frequency have major influence on the PA amplitude and phase shift. The behaviour of the PA amplitude and phase shift changes dramatically at phase transition regions. However, the N–SmA transition temperature remains unaffected and depends significantly only on scanning rate because of the thermal lag. So calibration with zero scanning rate is necessary. In Fig. 6, the PA amplitude and phase shift of two laser beam powers of 5 and 34 mW are shown in the region of N–SmA transition. The measurement was carried out with a heating and cooling rate of 5 K min^{-1} and with a frequency f=63 Hz. Only heating curves are presented for the sake of clarity. It was found that the change of laser beam power by a factor of 7 actually did not change the N–SmA transition temperature. The measured N–SmA transition temperature at 341 K is close to the literature value, the magnitude of the step in the PA amplitude decreased approximately by a factor of 2. Furthermore, it seems that I–N transition moves to higher temperatures with a decrease of the laser beam power, but it is difficult to estimate this effect exactly due to the noise in the signal at low beam powers.

The results show that the N–SmA transition of the liquid crystal 8OCB is suitable for temperature calibration on heating and cooling when applied to variable temperature PA measurements. But it is still an open question why a step in PA amplitude is observed and not a peak.

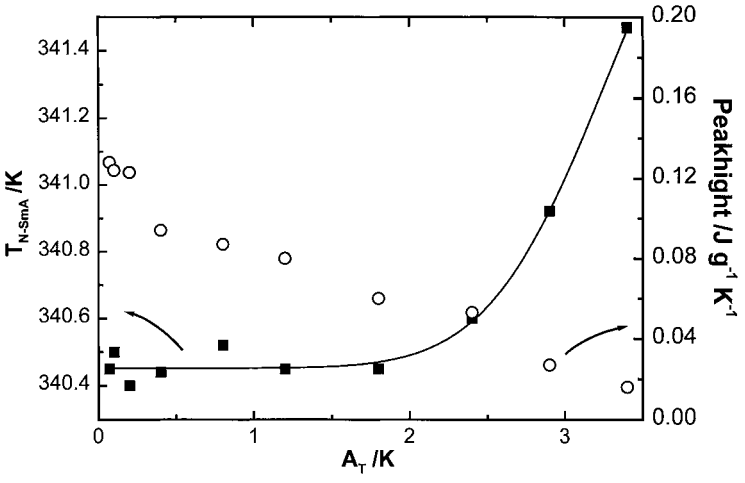

Fig. 7. ■ peak temperature T_{N-SmA} and ○ peak height of the nematic–smectic-A transition of 8OCB as a function of modulation amplitude T_A (PE DSC-7; 0.07 K$\leq T_A \leq$3.4 K; t_p=50 s; q_0=0.4 K min^{-1}; m_p=12 mg).

3.4. TMDSC

In TMDSC [6] parameters such as temperature amplitude, modulation period, underlying heating rate, sample mass and purge gas can be chosen over a rather wide range. In this work, the N–SmA transition of the liquid crystal 8OCB was studied to demonstrate how the temperature calibration of the TMDSC is influenced by the first three of these parameters [19].

The temperature amplitude was varied between 0.07 and 3.4 K keeping all the other parameters fixed as given in the legend of Fig. 7. As a result, the peak temperature was not affected for temperature amplitudes lower than 2 K. For temperature amplitudes higher than 0.2 K there was a considerable peak broadening, which can be seen from the decreasing peak height. An amplitude of T_A=0.2 K equals a peak to peak temperature difference of about 0.4 K, which is of the same order of magnitude as the peak width of about 0.5 K. Thus, the peak becomes significantly wider if the temperature modulation passes most of the transition during one heating or cooling cycle. As a

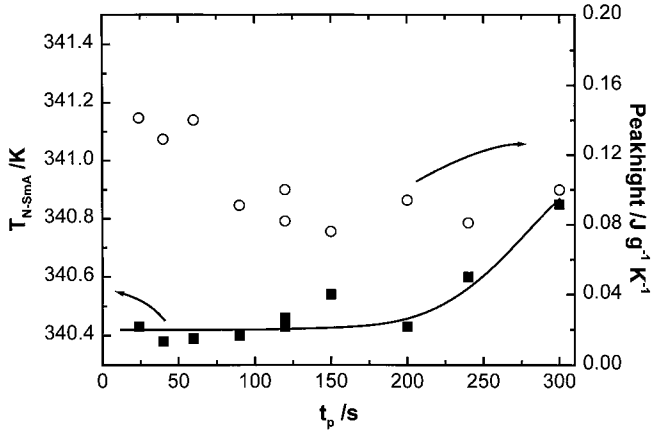

Fig. 8. ■ peak temperature T_{N-SmA} and ○ peak height of the nematic–smectic-A transition of 8OCB as a function of modulation period t_p (PE DSC-7; 12 s$\leq t_p \leq$300 s; T_A=0.2 K; q_0=0.4 K min^{-1}; m_p=12 mg).

consequence, the influence of the non-linear response cannot be neglected [30].

To study the effect of the influence of the modulation period, the modulation period was varied over the range 12–300 s keeping the other parameters fixed as shown in Fig. 8. As a result, the peak temperature is not significantly influenced for periods shorter than 200 s but for periods longer than approximately 60 s the peak becomes broader and suppressed. Due to the underlying heating rate of q_0=0.4 K min^{-1} almost the whole peak is passed within one modulation period for periods longer than 60 s. For these periods, the well known prerequisite for accurate TMDSC measurements — to perform at least some modulations during the effect under investigation to fulfill condition of stationarity [30] — is not satisfied which results in a loss of information.

The influence of the underlying heating rate can be studied for both conventional DSC and TMDSC and measurements were made in both these modes [19]. Thermal lag must be taken into account in both cases.

To summarise the results from TMDSC in Fig. 9, curves obtained under very different measuring conditions are shown. Peak position and peak shape are only slightly affected by the different parameters as long as condition of linearity and stationarity are fulfilled [30]. In TMDSC underlying heating rate (thermal lag) is important for temperature calibration just as it is in the DSC case. If a thermal lag compensation is included in the DSC software care must be taken when operated in TMDSC mode, for details see [19].

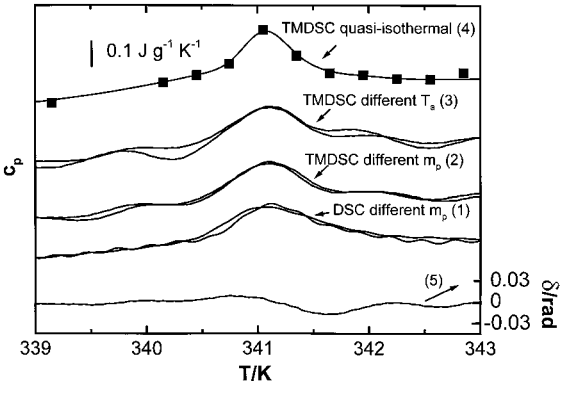

Fig. 9. Specific heat capacity c_p from conventional DSC and TMDSC measurements on 8OCB in the nematic smectic-A transition region. (1) DSC measurements (PE DSC-7) at q=10 K min^{-1} and different sample masses; m_p=4 and 12 mg. (2) TMDSC measurements (PE DSC-7) with T_A=0.2 K; t_p=60 s; q_0=0.4 K min^{-1}; and different sample masses; m_p=4 and 12 mg. (3) TMDSC measurements (PE DSC-7) with t_p=60 s; q_0=0.4 K min^{-1} m_p=4 mg and different modulation amplitudes; T_A=0.1 and 0.2 K. (4) Quasi-isothermal TMDSC measurements (Setaram DSC 121) with T_A=0.1 K; t_p=600 s; q_0=0; m_p=21 mg. (5) Phase angle from a TMDSC measurement (PE DSC-7) with T_A=0.2 K; t_p=60 s; q_0=0.4 K min^{-1}; m_p=12 mg.

4. Conclusions

Temperature calibration of different types of temperature modulated calorimeters can be performed with weak second-order phase transitions. As Fourier analysis is used when calculating different quantities in TMC it is essential to show that linear behaviour holds for the whole measuring system, including the transition itself. Proof of linearity can be obtained from a study of the effects of temperature amplitude on heat capacity. The nematic to smectic-A transition of 8OCB yields linear response for small temperature amplitudes ($T_A \leq 0.2$ K) because of the relatively small width (0.5 K) of this transition. Generally, such a transition can be used for temperature calibration in TMC.

In all cases when temperature scan measurements are performed, lag effects must be considered. As well known from DSC measurements, thermal lag results in a shift of the temperature scale. In TMC, as shown in the example of the AC calorimeter, time lag due to data treatment (e.g. the time constant of the lock-in amplifier) yields an analogues shift. Therefore, in TMC calibration of the thermometer and consideration of thermal lag (temperature gradient) is not enough for precise temperature calibration.

For temperature calibration of temperature modulated calorimeters using the liquid crystal 8OCB we recommend:

1. Determine the nematic to smectic-A transition temperature of the sample batch by an independent method, e.g., DSC or adiabatic calorimeter. If an underlying heating or cooling rate is applied, thermal lag effects must be taken into account. The transition temperature has to be extrapolated to zero heating rate [10].

2. Perform measurements with the calorimeter to be calibrated. Again, if an underlying heating or cooling rate is applied, extrapolation to zero heating rate is necessary. The possible difference between transition temperatures of 8OCB from both measurements can be used for a single point temperature calibration of the calorimeter. The procedure should be repeated with another suitable sample with a weak second-order phase transition so that the temperature range of interest is covered.

Acknowledgements

The authors gratefully acknowledge financial support by the European Commission, grant 15CT96-0821 and Merck KGaA, Darmstadt, for supplying the 8OCB substance.

References

[1] N.O. Birge, S.R. Nagel, Phys. Rev. Lett. 54 (1985) 2674–2677.
[2] N.O. Birge, S.R. Nagel, Rev. Sci. Instrum. 58 (1987) 1464–1470.
[3] N.O. Birge, P.K. Dixon, N. Menon, Thermochim. Acta 304/305 (1997) 51–66.
[4] J. Thoen, C. Glorieux, Thermochim. Acta 304/305 (1997) 137–150.
[5] P. Sullivan, G. Seidel, Phys. Rev. 173 (1968) 679–685.
[6] H. Gobrecht, K. Hamann, G. Willers, J. Phys. E: Scientific Instruments 4 (1971) 21–23.
[7] S. Weyer, A. Hensel, J. Korus, E. Donth, C. Schick, Thermochim. Acta 304/305 (1997) 251–255.
[8] B. Wunderlich, Y.M. Jin, A. Boller, Thermochim. Acta 238 (1994) 277–294.
[9] C. Schick, G.W.H. Höhne (Eds.), Special issue 'Temperature Modulated Calorimetry', Thermochim. Acta 304/305 (1997).
[10] S.M. Sarge, W. Hemminger, E. Gmelin, G.W.H. Höhne, H. Cammenga, W. Eysel, J. Thermal Anal. 49 (1997) 1125–1134.
[11] M.J. Richardson, N.G. Savill, Thermochim. Acta 12 (1975) 213–220.
[12] M.J. Richardson, The application of differential scanning calorimetry to the measurement of specific heat, in: K.D. Maglic, A. Cezairliyan, V.E. Pelewtsky (Eds.), Compendium of Thermophysical Property Measurement Methods, Plenum Press, New York, 1992, Chapter 18, p. 519–545.
[13] T. Ozawa, K. Kanari, Thermochim. Acta 253 (1995) 183–188.
[14] B. Wunderlich, Thermal Analysis, Academic Press, New York, 1990.
[15] W. Hemminger, G. Höhne, Calorimetry, Verlag Chemie, Weinheim, 1984.
[16] C.W. Garland, G.B. Kasting, K.J. Lushington, Phys. Rev. Lett. 43 (1979) 1420–1423.
[17] D.L. Johnson, C.F. Hayes, R.J. deHoff, C.A. Schantz, Phys. Rev. B 18 (1978) 4902–4912.
[18] A. Zywocinski, S.A. Wieczorek, J. Stecki, Phys. Rev. A 36 (1987) 1901–1907.
[19] A. Hensel, C. Schick, Thermochimica Acta 304/305 (1997) 229–237.
[20] D. Lörinczy, J. Belagyi, Biochem. Biophys. Res. Com. 217 (1995) 592–598.
[21] G.W.H. Höhne, J. Schawe, C. Schick, Thermochim. Acta 221 (1993) 129–138.
[22] U.G. Jonsson, O. Andersson, A. Fransson, Thermochim. Acta 347 (2000) 45–51.
[23] A.A. Minakov, Thermochim. Acta 304/305 (1997) 165–170.
[24] Ts. Vassilev, Ts. Velinov, I. Avramov, S. Surnev, Appl. Phys. A 60 (1995) 1–6.
[25] M. Gateshki, K. Brunzalov, Ts. Vassilev, in preparation.
[26] U.G. Jonsson, O. Andersson, Meas. Sci. Technol. 9 (1998) 1873–1885.
[27] A.A. Minakov, Yu.V. Bugoslavsky, C. Schick, Thermochimica Acta 317 (1998) 117–132.
[28] Ts. Vassilev, Thermochim. Acta 347 (2000) 53–61.
[29] M. Gateshki, K. Brunzalov, Ts. Vassilev , Science Communication, Vol. 1, Proc. Conf. Defectoscopy 98, Sozopol 10–12 June 1998, p. 23.
[30] M. Merzliakov, C. Schick, Thermochim. Acta 330 (1999) 55–64.